Building Single Molecules from Single Atoms

A DISSERTATION PRESENTED
BY
YICHAO YU
TO
THE DEPARTMENT OF PHYSICS

IN PARTIAL FULFILLMENT OF THE REQUIREMENTS
FOR THE DEGREE OF
DOCTOR OF PHILOSOPHY
IN THE SUBJECT OF
PHYSICS

HARVARD UNIVERSITY
CAMBRIDGE, MASSACHUSETTS
MARCH 2021

Thesis advisor: Professor Kang-Kuen Ni Yichao Yu

Building Single Molecules from Single Atoms

Abstract

Contents

Acknowledgments

,

0

Introduction

1

Apparatus

1.1 Cooling and optical pumping beams

(MOT, OP, fiber back reflection)

(Mention Na Raman beam to be covered in later chapter?)

1.2 Tweezer and imaging

1.3 Molecular Raman frequency generation

(beam path, calibration)

2

Computer control of the experiment

2.1 Overall structure

2.2 Frontend

(Abstraction) (Backward compatibility) (Flexibility) (Text based/version control friendly)

2.3 Backends

(communication protocol) (IR)

2.3.1 FPGA backend

(clock generation) (pulse merging) (compression)

2.3.2 NiDAQ backend

(Variable clock)

2.3.3 USRP backend

(SIMD)

2.4 Automation of scan

(Scan requirement) (Combination of scans) (Scope/nested structure)

2.5 Summary and Outlook

(new backend/SPCM) (native code generation, auto vectorization) (dynamic logic and dependency tracking/optimization)

3

Raman sideband cooling

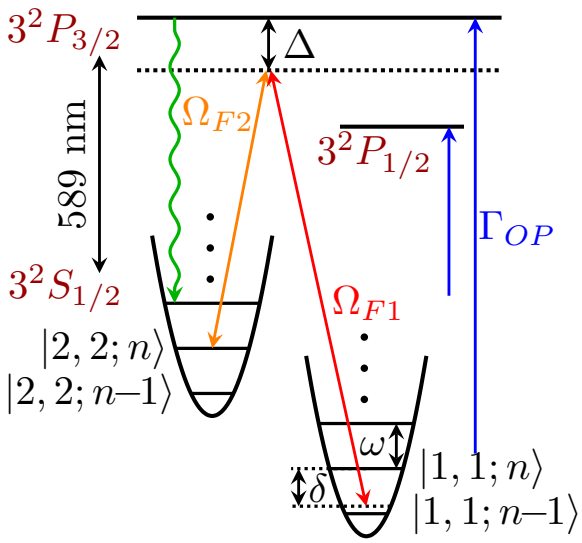

Figure 3.1: Single Na atom Raman sideband cooling scheme. The Raman transitions between $|2,2;n\rangle$ and $|1,1;n+\Delta n\rangle$ have a one-photon detuning $\Delta = 75$ GHz below the $3^2S_{1/2}$ to $3^2P_{3/2}$ transition. Two-photon detuning, δ, is defined relative to the $\Delta n = 0$ carrier transition. For optical pumping, we use two σ^+ polarized transitions, one to pump the atom state out of $|1,1\rangle$ via $3^2P_{3/2}$ and one to pump atoms out of $|2,1\rangle$ via $3^2P_{1/2}$ to minimize heating of the $|2,2\rangle$ state.

3.3 Setup

3.2

3.4 Challenge with large Lamb-Dicky parameter

3.3

3.5 Solution: High order sidebands

3.4

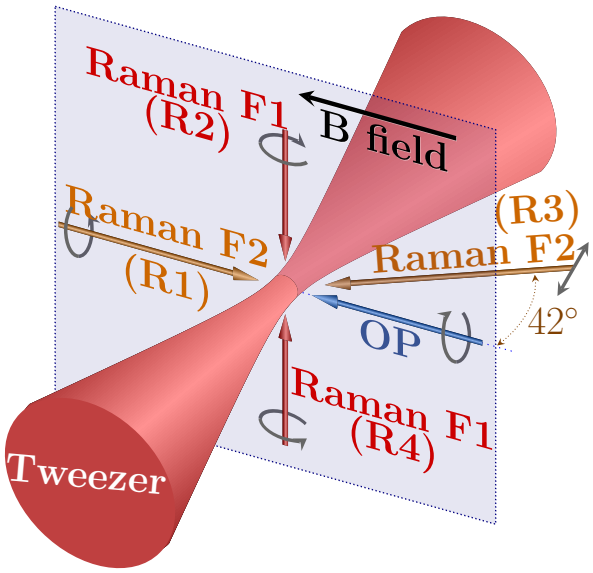

Figure 3.2: Geometry and polarizations of the Raman and optical pumping beams relative to the optical tweezer and bias magnetic field. Raman beams R1 and R4 address the radial x-mode. R1 and R2 address the radial y-mode. R3 and R4 address the axial z-mode, where the beams also couple to radial motion, but this coupling can be neglected when the atoms is cooled to the ground state of motion.

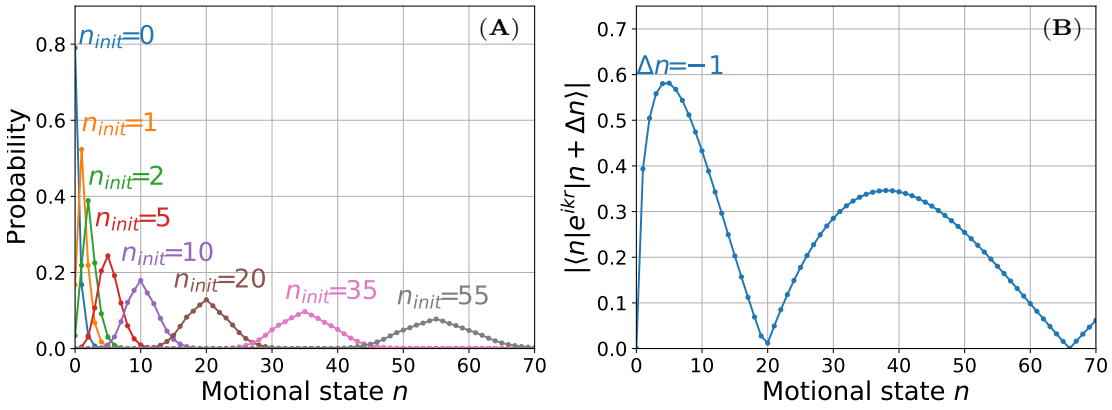

Figure 3.3: Optical pumping motional-state redistribution and Raman coupling for large LD parameters for the axial direction (z). The range plotted covers 95% of the initial thermal distribution. (A) Motional state distribution after one OP cycle for different initial states motion, n_{init}. Due to photon-recoil and the large LD parameter, $\eta_z^{\text{OP}} = 0.55$, there is a high probability of n changing. (B) Matrix elements for Raman transition on the first order cooling sideband deviate from $\sqrt{n}$ scaling with multiple minima.

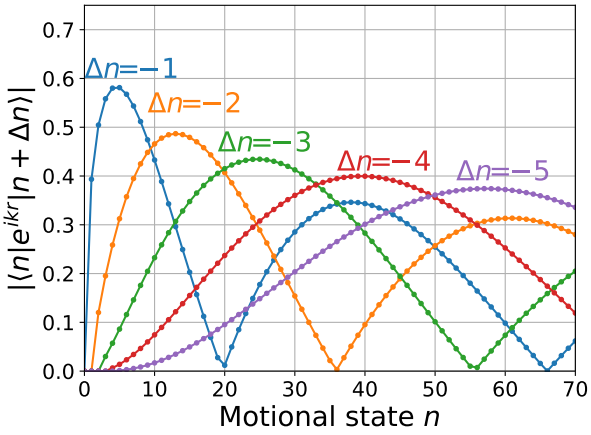

Figure 3.4: Matrix elements for Raman transition including high order sidebands. During cooling, we utilize the fact that high motional states couple most effectively to sidebands with large $|\Delta n|$ in order to overcome the issue with variation and dead zone in the coupling strengths.

3.6 Solution: Simulation based optimization

3.5

3.7 Cooling performance

3.6 3.7

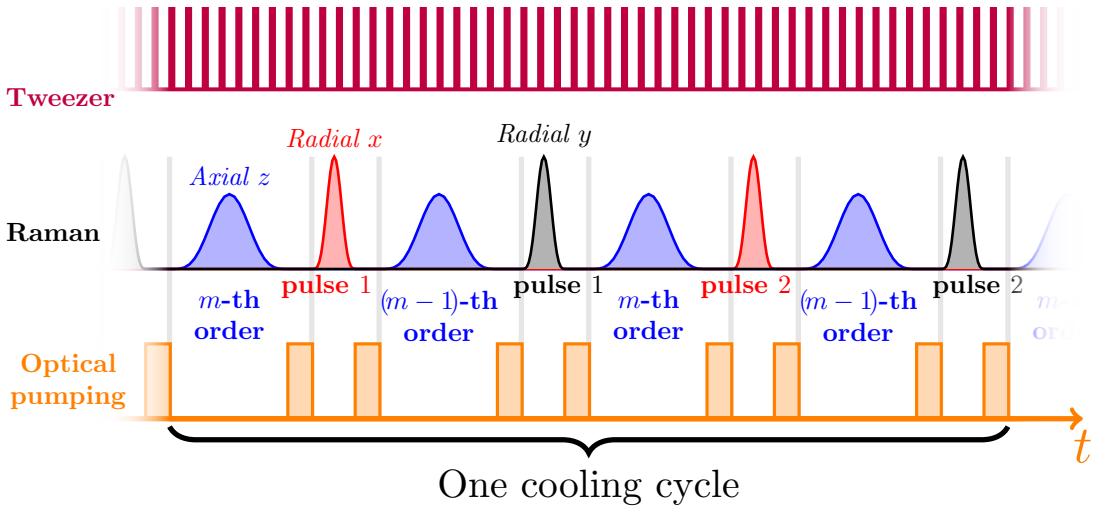

Figure 3.5: Schematic of the cooling pulse sequence. The tweezer is strobed at 3 MHz to reduce light shifts during optical pumping. Each cooling cycle consists of 8 sideband pulses. The four axial pulses address two sideband orders. The two pulses in each radial direction either address $\Delta n = -2$ and $\Delta n = -1$ or have different durations to drive $\Delta n = -1$, at the end of the cooling sequence when most of the population is below $n = 3$. The Raman cooling and spectroscopy pulses have Blackman envelopes to reduce off-resonant coupling, while the measurement Rabi pulses in Fig. 3.7 have square envelopes to simplify analysis.

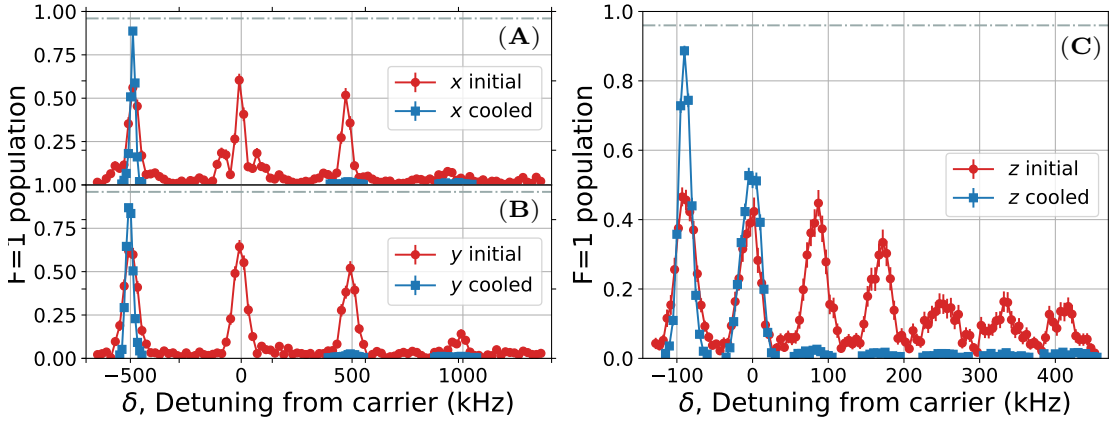

Figure 3.6: Raman sideband spectra for (A) x, (B) y, (C) z axis before (red circle) and after (blue square) applying Raman sideband cooling sequence. The height of the cooling sidebands (positive detuning) are strongly suppressed after cooling which suggests most of the atoms are cooled to the motional ground state in the trap.

Figure 3.7 *(following page)*: Rabi flopping on radial axis x (A) carrier and (B) $\Delta n_x = 1$ sideband, radial axis y (C) carrier and (D) $\Delta n_x = 1$ sideband, axial axis z (E) carrier and (F) $\Delta n_x = 1$ sideband, before (red circle) and after (blue square) Raman sideband cooling.
Solid lines (both red and blue) in all plots are fits to a Rabi-flopping that includes a thermal distribution of motional states as well as off-resonant scattering from the Raman beams.
The blue lines correspond to a ground state probability of (A-D) 98.1% along radial axis and (E-F) 95% along the axial axis after cooling. The red lines correspond to a thermal distribution of 80 μK before RSC. The horizontal dashed lines in all the plots correspond to the $4\ \%$ probability of imaging loss.
The green dashed line in (F) includes the additional decoherence due to a fluctuation of the hyperfine splitting of magnitude 3 kHz. We see that the decoherence effect is strongest for the post-cooling data on the axial $\Delta n_z = 1$ sideband where the Rabi frequency is the lowest.

Figure 3.7: (continued)

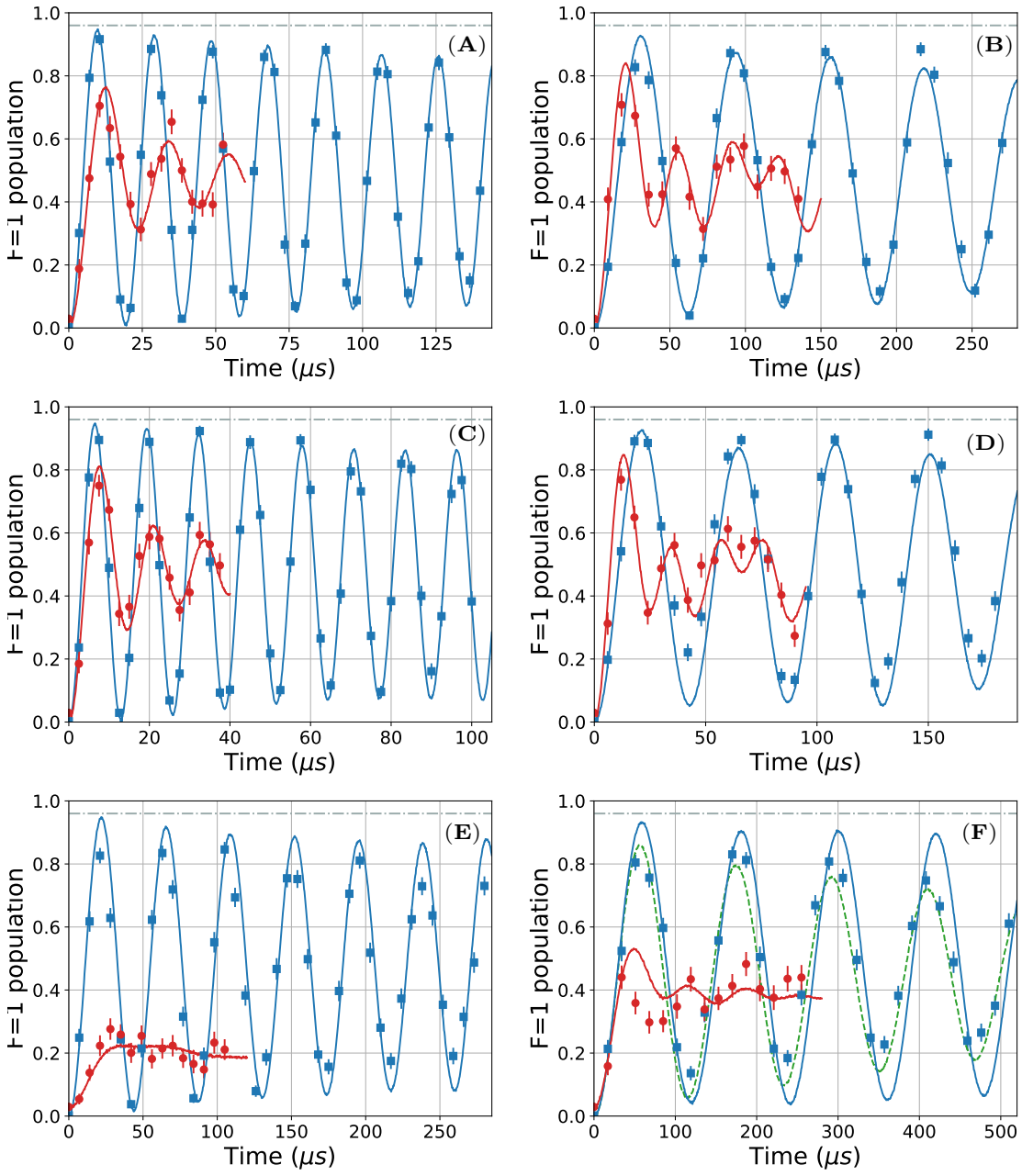

4

Interaction of single atoms

4.1 Scattering length

(Importance/relation with binding energy etc.)

4.2 Energy levels of two interacting atoms in an anisotropic trap

4.3 Interaction shift spectroscopy

(motional sideband, scattering length result)

4.4 Summary and Outlook

(Motional state selection)

5

Photoassociation of single atoms

5.1 Energy levels

5.2 Effect of the trap

(light shift, broadening)

5.3 Photoassociation spectroscopy

(v=0, 12, 14, etc)

6

Two-photon spectroscopy of NaCs ground state

(N=2, different HF states)

7

Coherent optical creation of NaCs molecule

8

Conclusion